Carbon-Aware Operation of Resilient Vertical Farms in Active Distribution Networks

Arash Farokhi Soofi, *Student Member, IEEE* and Saeed D. Manshadi, *Member, IEEE*

***Abstract*—Vertical farming is an emerging sustainable solution to enhance the resilience of the food supply and mitigate the carbon emissions of the agriculture sector amidst population growth, geopolitical risks, and climate change concerns. The proximity of food production to consumers enhances food supply resilience. Besides, the potential to leverage renewable resources to energize Vertical Farms (*VF*s) paves the way to mitigating their food carbon emissions. At the same time, *VF*s will introduce new challenges and opportunities within Active Distribution Networks (*ADN*s). While the electricity demand will increase within the *ADN*, the flexibility in *VF*'s electricity demand provides system operators with demand-side management opportunities. This paper proposes a model to explore the demand of various systems within a *VF* and their coordination with other assets within the *ADN*, such as Electric Vehicles (*EV*s) and photovoltaic (*PV*) systems. To this end, a framework to procure the optimal operation schedule of *VF*s under demand and solar generation uncertainties with convexified AC power flow constraints is presented. It is shown that the proposed framework also enhances the dispatchability of renewable Distributed Energy Resources (*DER*s). The formulated two-stage robust optimization problem is reformulated as a Mixed-Integer Second-Order Cone Programming (*MISOCP*) problem to be solved by reliable off-the-shelf solvers. It is shown that the demand response of *VF*s can mitigate the carbon emissions of the electricity and agriculture sectors by up to 70% and decrease the operation cost of the electricity network by 10% for the IEEE-33 bus system compared to utilizing an inflexible schedule for *VF*s.**

***Index Terms*—demand response, distribution network, vertical farms, uncertainty, sustainable communities.**

NOMENCLATURE

Sets

$\mathcal{D}/\mathcal{D}_i$	Set of all loads / loads connected to bus i
$\mathcal{E}/\mathcal{E}_i$	Set of all *EV* fleets / fleets connected to bus i
$\mathcal{F}/\mathcal{F}_i$	Set of all vertical farms / *VF*s connected to bus i
$\mathcal{G}/\mathcal{G}_i$	Set of all feeders connected to the network / bus i
$\mathcal{S}/\mathcal{S}_i$	Set of all *PV*s / *PV*s connected to bus i
$\mathcal{L}_f$	Set of all levels of vertical farm f
$\mathcal{T}$	Set of time horizon
$\mathcal{Z}$	Set of electricity generation resources
δ_i	Set of adjacent buses to bus i

Variables

c, s	Lifting operator terms of *SOCP* relaxation
e_i, f_i	Real/imaginary part of voltage phasor of bus i
E_e^t	Energy of the fleet of *EV* e at time t (MWh)
$I_{(.),f}^t$	Status of systems within *VF* f at time t
P_s^t	Real power dispatch of solar s at time t (MW)
$P_{e,t}^c$	Real charging power of *EV* fleet e at time t (MW)
$P_{f,li/ir}^t$	Real power demand of the lighting/irrigation system of *VF* f at time t
$P_{l,f}^{a,t,+/-}$	Real power demand of air conditioniner of level l of *VF* f at t working in heating/ cooling mode
$P_{l,f}^{X,t}$	Exchange heating power of level l of farm f at t
$P_{l,f}^{h,t}$	Real power demand of the dehumidification system of level l of *VF* f at time t
$Q_{f,li/ir}^t$	Reactive power demand of the lighting/ irrigation system of *VF* f at time t
$Q_{l,f}^{a/h,t}$	Reactive power demand of the air conditioner/ dehumidifier of level l of *VF* f at time t
P_f^t, Q_f^t	Real/reactive power demand of *VF* f at time t (MW/MVAR)
P_g^t, Q_g^t	Real/reactive power dispatch of generation unit g at time t (MW/MVAR)
P_{ij}^t, Q_{ij}^t	Real/reactive power flow between bus i and j at time t (MW/MVAR)
$\theta_{l,f}^t$	Temperature of level l within *VF* f at time t (K)
$\varsigma_{l,f}^t$	Absolute humidity of level l of farm f at time t $(\frac{lit}{m^3})$
μ,λ	Dual variables

Parameters

A_l^f	The cultivable area of level l within *VF* f (m^2)
$A_{l,f}^w$	The surface of walls of level l within *VF* f (m^2)
B/G	Susceptance / conductance matrix (S)
BoU	Budget of uncertainty $(\%)$
C_a	The specific heat capacity of air $(\frac{MWh}{kgK})$
$C_E^{z,t}$	Carbon emissions of electricity generation z at t $(\frac{MT}{MW})$
g	The gravitational force $(\frac{m}{s^2})$
i_l^f	The required LED light intensity for level l of vertical farm f (lux)
$K_{l,f}^w$	Thermal conductivity of level l walls within *VF* f $(\frac{MW}{mK})$
$\overline{p_e^c}$	Maximum charging power of fleet of *EV*s e (MW)
$p_D^{t,0}$	Forecasted real power of load d at time t (MW)
p_D^t	Real power demand of load d at time t (MW)
$\overline{p}_s^{t,0}$	Forecasted available solar power for *PV* s at time t (MW)
$\overline{p}_s^t$	Available solar power for *PV* s at time t (MW)
q_D^t	Reactive power of load d at time t (MVAR)
$p_{e,t}^{tr}$	Traveling power consumption of *EV* e at time t (MW)
$p_{l,f}^t$	Fertilization demand of level l of farm f at time t (MW)
p_w	Electricity demand of the dehumidifier to remove 1 liter water form the air (MW)
T_h	Total seconds in an hour (sec)

Arash Farokhi Soofi is with University of California San Diego, LaJolla, CA, 92093, USA, and San Diego State University, San Diego, CA, 92182 USA. Saeed D. Manshadi is with San Diego State University, San Diego, CA, 92182 USA. e-mail: afarokhi@ucsd.edu; smanshadi@sdsu.edu.

τ_l^f	The required lighting hours for level l of *VF* f (h)
τ_{ir}^f	The required hours to irrigate *VF* f (h)
m_w^f	Total water demand of *VF* f in a day (kg)
$W_{l,f}^{e,t}$	Evaporated water from crops of level l within *VF* f at time t (lit)
$X_{l,f}^w$	The thickness of walls of level l within *VF* f (m)
γ_e	Inverter efficiency of *EV* fleet e
Δ_h^f	The height *VF* f (m)
ϵ_l	The efficacy of the LED lamps ($\frac{lux}{MW}$)
η_p^f	The efficiency of water pump p in *VF* f (%)
η_a^f	The efficiency of air conditioning systems of *VF* f
θ_{out}^t	Outside temperature of *VF* at time t (K)
ρ_z^t	Share of generation type z at time t
α_t	Time-of-Use cost of electricity at time t ($\frac{\$}{MWh}$)

I. Introduction

The growth in the world's population will lead to fundamental changes in energy and food security. The world population is predicted to reach 9 billion by 2050 [1], and 80% of the population will reside in urban areas [2]. Thus, the demand for fresh food in cities will grow. Climate change concerns over deforestation and geopolitical conflicts will lead to more limited access to agricultural [3]. Thus, an emerging challenge is to present a sustainable, efficient, and cost-effective food supply chain. The growing trend of "vertical farming" as a potentially sustainable food supply solution [4] aims to address several challenges, including but not limited to shedding the restrictions on agricultural products due to seasonal weather patterns, natural disasters, temperature changes [5], water supply, and irradiance intensity, overcoming transportation challenges [6], and the need to significantly enhance yields [7]. The *VF* concept envisions the sprawling crop farms of old condensed into much smaller factory-like sites where conditions can be *optimized and yields are remarkably increased* [8], [9]. Vertical farming is a concept that involves cultivating plants on vertically inclined surfaces, where it is *resilient* against weather-related distress and geopolitical disruptions impacting the food supply chain network. Some argue that the ultimate goal of vertical farming is to provide fresh food for the entire population of the world without concern for climate change and disasters[10].

Transportation, agriculture, and the electricity sectors are among the largest global emitters of greenhouse gases, and they can account for 70% of the global greenhouse gas emissions by 2050 [11]. The Paris agreement in 2015 set out a desire to limit the global temperature rise to 1.5^oC above pre-industrial levels. Yet, based on the current trends in emissions and national policy commitments, the Paris targets are in jeopardy [12]. Utilizing vertical farms can mitigate the carbon emissions of the agriculture and transmission sectors by eliminating the need for harmful pesticides, which account for 33% of the total indirect carbon emissions of farm products [13], decreasing the food miles traveled [14], eliminating the usage of combustion engine machinery, (e.g., tractors), and increasing the yield of crops [1]. In [15], the authors present a roadmap to decrease the carbon emissions of the agricultural sector. This paper aims to illustrate how the increase in the penetration level of *VF*s will contribute to a reduction in the carbon emissions of smart communities.

With the projected increase in the utilization of *VF*s in urban areas, investigating the challenges and opportunities of utilizing these new loads for the electricity grid plays a vital role in the operation and planning problems of the electricity network. Thus, presenting a demand-side model to present the performance of different systems in a *VF* is the key to studying those challenges and opportunities. The systems that should be considered within a *VF* are 1) lighting; 2) irrigation and fertilization; 3) air conditioning; and 4) dehumidification system [4], as presented in Fig. 1. Coordinating the energy consumption of these loads with the operation of the electricity *ADN* can enhance the operational planning characteristics of the network in terms of renewable dispatchability and demand response. Currently, there is a *gap* in the literature to investigate the demand response potentials of various systems within a *VF* as a flexible asset to the smart grid. This paper presents a model exploring different aspects and ambient features of a *VF* to become a flexible asset to the smart grid. The proposed model for *VF*s is utilized for coordinating the flexible demand of *VF*s with other assets within the *ADN* to enhance the resilience of food and energy supply. This paper shows that utilizing *VF*s as the main resource to meet the food demand will consume about 30% of the share of the electricity demand. The future smart grid is

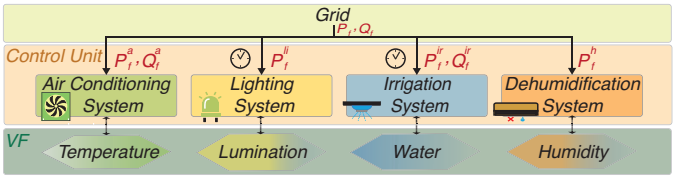

Fig. 1: Control unit and electricity demand of different systems within a vertical farm

expected to include independent entities, such as prosumers, who will plug in their generation or consumption devices at their discretion. The penetration level of uncertain *DER*s in the power system is increasing. Particularly, increasing the penetration level of *EV*s within the *ADN* will deteriorate the power quality [16]. A practical tool to address these challenges is demand response. Demand response refers to encouraging end-users through a specific tariff or program to change their normal electricity consumption patterns, i.e., consume less power during peak times or shift their electricity demand to off-peak hours to flatten the demand curve [17]. Demand response transforms consumers into players with a more active role in energy management by leveraging the potential flexibility in electricity loads [18]. Several flexible demand entities, including data centers[19], *EV* charging stations[20], [21], residential *EV*s [22], cooling and heating loads [23], and residential loads [24] are presented as demand-responsive loads in the literature to remedy the challenges raised by *DER* uncertainty within the *ADN*. Besides, several authors have modeled the air conditioning systems within residential loads with the focus of utilizing the model of air conditioning systems for demand response [25]. However, this paper models the irrigation and lighting systems within a *VF* as demand-

responsive assets. The numerous operational advantages of demand response are enumerated in the literature and are also applicable to *VF*s. First, *VF* demand response could mitigate the difference between peaks and valleys of power demand. Second, adjusting the internal schedules of the *VF* could enhance the dispatchability of renewable *DER*s, similar to those achieved by utilizing *EV*s [26]. This paper presents the model of *VF*s as a demand-responsive asset in coordination with uncertain *DER*s such as *EV*s and *PV* systems within an *ADN*. Several control systems, including lighting and irrigation systems, can operate as shiftable loads within a *VF*. To ensure proper crop yield and growth, the air conditioning and dehumification systems are constantly controlled to maintain temperature and humidity within the desired range. Scheduling *VF* based on the unit cost of electricity aims to minimize their operation costs. Besides, their carbon emissions may be mitigated by operating during hours of abundant renewable energy.

This paper aims to address the following questions: *What would be the benefit of coordination between the electricity demand of systems within* VF*s and other assets within the* ADN*? Can the flexibility of the demand within a* VF *provide utilities with demand-side management opportunities to enhance renewable dispatchability? Is the electricity distribution network ready for the emerging electricity demand of* VF*s?*The main contributions of this paper are listed as follows.

- The model of various systems within a vertical farm is presented and formulated as a demand-responsive asset. It is shown that coordinating *VF*s with *DER*s and other demands within the *ADN* enhances the dispatchability of renewable *DER*s, decreases the unfortunate renewable generation curtailments, and thus decreases the overall carbon emissions and operating cost of the *ADN*.
- A framework is presented to examine the preparedness of *ADN* for various scenarios of *VF*s penetration level considering demand and solar generation uncertainties, where the objective function is carbon emissions minimization or operation cost minimization. Here, demands within the *VF*s across the *ADN* are scheduled over a selected set of worst-case uncertainty realizations. Furthermore, it is illustrated that coordinated scheduling of *VF*s mitigates the adverse impact of uncertainties in renewable generation and demand on the operation of *ADN*.
- The impact of utilizing *VF*s, as a sustainable food supply solution, on the carbon emissions of the electricity and agriculture sectors is evaluated. Besides, the performance of the proposed framework on other emerging challenges within the *ADN* including the increase in electricity demand of EVs due to the push toward transportation electrification, is presented.

II. Problem Formulation

In this paper, first, models of different systems in *VF*s are suggested. Then, the optimal operation schedule of shiftable systems within *VF*s is proposed and coordinated with other assets within the *ADN*. The optimal operation scheduling problem for the *VF*s considering the uncertainties of demand and solar generation units is a two-stage robust optimization problem. Here, the schedule of the irrigation and lighting systems within a VF are here-and-now decision variables that are procured in the first-stage problem. Each type of crop requires a specific *daily* intake of light and water to ensure optimal growth, which must be satisfied. The power dispatch of the feeder bus, the utilized solar generation, demand of air conditioning and dehumidification systems, and the served demand are the wait-and-see decision variables, which are determined based on the uncertainty realization in the second-stage problem. Here-and-now decision variables are the first-stage decisions that will be made at the time for deciding the daily schedule of the shiftable systems within *VF*s. Once the decisions are made, they cannot be adjusted during the operation period of the problem. The wait-and-see decision variables are the second-stage decisions, which could change given the realization of uncertain variables. Therefore, the main criterion to distinguish them is the necessity of making the decision at the time of determining the daily schedule for the *VF*. Two different objectives are considered for the optimal scheduling problem, which is a two-stage robust optimization problem: carbon emissions minimization and operation cost minimization.

A. Objective Function

The presented discussion aims to address the operation preferences of cost minimization and carbon emission minimization.

1) Carbon emissions minimization problem: The objective function of the optimal operation scheduling problem for *VF*s with respect to carbon emissions is proposed in (1). The first-stage problem minimizes the operation carbon emissions of the shiftable systems within *VF*s by procuring the optimal operation schedule of *VF*s. As concerned in the second-stage problem, the carbon emissions of the *ADN* and *VF*s depends on the generation mix, which consists of various resources, ρ_z^t, (e.g., natural gas, renewable resources, imports of connected transmission networks, etc.), the total power dispatch of the feeder at time t, and the corresponding carbon emissions of each source to generate 1 p.u. of electricity, $C_E^{z,t}$, at time t. The carbon emissions of the generation mix is changing over the operation horizon. For instance, the carbon emissions of the generation mix is low during sunny hours due to the increase in the share of solar generation units, and it is high due the to low participation of renewable generation during the night. The first term in the carbon minimization function (1) presents the shiftable carbon emissions of the irrigation and lighting systems of *VF*s over a time horizon T, respectively. The real power demand of the irrigation and lighting systems, i.e., shiftable systems within *VF*, depends on the first-stage binary decision variables, the status of lighting and irrigation systems ($I_{l,f}^{li,t}, I_f^{ir,t}$), at time t. The electricity demand of the irrigation and fertilization systems of farm f at time t depends on the status of the irrigation system, the total water demand of *VF* f in a day, m_w^f, the height of the farm, Δ_h^f, the gravitational force,g, the efficiency of the water pumps, and the total number of irrigation periods, τ_{ir}^f, as well as the fertilization demand at each irrigation period. The electricity power demand of the lighting system of *VF* f at time t depends on the required LED light intensity for the growth of crops at each level,

i_l^f, the cultivated area, A_l^f, the efficacy of LEDs, ϵ_l, and the status of the lighting system at level l of farm f at time t, $I_{l,f}^{li,t}$. The last term presents the second-stage carbon emissions minimization of the *ADN* over the worst-case realization of uncertain variables (i.e., demand and solar availability).

$$\min_{I_{l,f}^{li,t}, I_f^{ir,t}} \sum_{t\in\mathcal{T}} \Bigg[\sum_{f\in\mathcal{F}} \sum_{z\in\mathcal{Z}} C_E^{z,t} \Bigg((\frac{m_w^f g \Delta_h^f}{\tau_{ir}^f T_h \eta_p^f} + \sum_{l\in\mathcal{L}_f} p_{l,f}^t) I_f^{ir,t} + \sum_{l\in\mathcal{L}_f} \frac{A_l^f i_l^f}{\epsilon_l} I_{l,f}^{li,t} \Bigg) \rho_z^t \Bigg] + \max_{p_D^t, \overline{p}_s^t} \min_{P_g^t} \sum_{t\in\mathcal{T}} \sum_{g\in\mathcal{G}} \sum_{z\in\mathcal{Z}} C_E^{z,t} P_g^t \rho_z^t \quad (1)$$

2) Operation cost minimization problem: The objective function of the optimal operation scheduling for *VF*s with the minimum operation cost is proposed in (2). The first two terms in (2) present the first-stage problem that minimizes the operation cost of the shiftable systems within *VF*s over $\mathcal{T}$. The operation cost of the *VF*s depends on the Time-of-Use (ToU) price of the electricity, α_t, and the real power demands of lighting and irrigation systems over $\mathcal{T}$. In the first-stage problem, the optimal schedule of the irrigation and lighting systems ($I_{l,f}^{li,t}, I_f^{ir,t}$) are procured to minimize the operation cost of *VF*s. The last term of the objective function presents the second-stage problem that minimizes the operation cost of *ADN* over $\mathcal{T}$ over the worst-case realization of uncertain variables (i.e., demand and solar generation).

$$\min_{I_{l,f}^{li,t}, I_f^{ir,t}} \sum_{t\in\mathcal{T}} \Bigg[\sum_{f\in\mathcal{F}} \alpha_t \Bigg((\frac{m_w^f g \Delta_h^f}{\tau_{ir}^f T_h \eta_p^f} + \sum_{l\in\mathcal{L}_f} p_{l,f}^t) I_f^{ir,t} + \sum_{l\in\mathcal{L}_f} \frac{A_l^f i_l^f}{\epsilon_l} I_{l,f}^{li,t} \Bigg) \Bigg] + \max_{p_D^t, \overline{p}_s^t} \min_{P_g^t} \sum_{t\in\mathcal{T}} \sum_{g\in\mathcal{G}} \alpha_t P_g^t \quad (2)$$

3) Joint cost and carbon emissions minimization problem: The joint cost and carbon emissions objective function of the optimal operation scheduling for *VF*s is proposed in (3), where the first two terms are for the first-stage problem and the last term represents the second-stage problem. Here, γ is the monetizing coefficient for carbon emissions.

$$\min_{I_{l,f}^{li,t}, I_f^{ir,t}} \sum_{t\in\mathcal{T}} \Bigg[\sum_{z\in\mathcal{Z}} (\alpha_t + \gamma C_E^{z,t} \rho_z^t) \sum_{f\in\mathcal{F}} \Bigg((\frac{m_w^f g \Delta_h^f}{\tau_{ir}^f T_h \eta_p^f} + \sum_{l\in\mathcal{L}_f} p_{l,f}^t) I_f^{ir,t} + \sum_{l\in\mathcal{L}_f} \frac{A_l^f i_l^f}{\epsilon_l} I_{l,f}^{li,t} \Bigg) \Bigg] + \max_{p_D^t, \overline{p}_s^t} \min_{P_g^t} \sum_{t\in\mathcal{T}} \sum_{g\in\mathcal{G}} \sum_{z\in\mathcal{Z}} (\alpha_t + \gamma C_E^{z,t} \rho_z^t) P_g^t \quad (3)$$

B. Vertical Farms Model

The model of systems within *VF*s is suggested in (4)-(8), which consists of lighting, irrigation and fertilization, air conditioning, and dehumidification systems. Note that in the proposed model, the electricity demand of the lighting and irrigation systems is 95% of the total *VF*s electricity demand [27]. The main advantage of *VF*s compared to conventional farming is their resilience against weather-related stress, as they maintain the crop's temperature within a threshold range of $27°C$ to $31°C$. In [28], the authors show that stress thermal time of more than 4000 $°C$-minutes decreases crop yield by more than 60%.

The total real and reactive electricity demand of *VF* f at time t is the sum of the real and reactive electricity demand of all the systems in the *VF* as proposed in (4a) and (4b), respectively. Note that the variable after each colon in front of constraints shows the dual variable corresponding to that constraint. The details of the model associated with each system within the *VF* are given as follows:

$$P_f^t = P_{f,li}^t + P_{f,ir}^t + \sum_{l\in\mathcal{L}_f} P_{l,f}^{a,t,+} + P_{l,f}^{a,t,-} + P_{l,f}^{h,t} : \lambda_P^{f,t} \quad (4a)$$

$$Q_f^t = Q_{f,ir}^t + \sum_{l\in\mathcal{L}_f} Q_{l,f}^{a,t} : \lambda_Q^{f,t} \quad (4b)$$

1) Lighting system: The model of the lighting system of *VF* f is suggested in (5). The electricity power demand of the lighting system of *VF* f at time t depends on the required LED light intensity for the growth of crops at each level, the cultivated area, the efficacy of LEDs, and the status of the lighting system at each level, as presented in (5a). The crops of each level of *VF* f need a specific duration of light per day to grow as presented in (5b).

$$0 \le P_{f,li}^t = \sum_{l\in\mathcal{L}_f} \frac{A_l^f i_l^f}{\epsilon_l} I_{l,f}^{li,t} : \underline{\mu}_{f,t}^{P_{li}}, \lambda_{f,t}^{P_{li}} \quad (5a)$$

$$\sum_{t\in\mathcal{T}} I_{l,f}^{li,t} = \tau_l^f \quad (5b)$$

2) Air conditioning system: The air conditioning system of level l of *VF* f is modeled in (6). The heating or cooling power of the air conditioning system to control the air temperature of level l of farm f is modeled in (6a). Here, $P_{l,f}^{a,t}$ is the heating or cooling power required at level l of farm f at time t. Note that $P_{l,f}^{a,t,+}, P_{l,f}^{a,t,-}$ are non-negative variables to model the absolute power demand of the air conditioning system working in heating and cooling modes. The exchange heating power, $P_{l,f}^{X,t}$, depends on the temperature difference of each level and outside, the walls' or glasses' thickness, area, and thermal conductivity, as presented in (6b). The maximum and minimum temperature of each level of the *VF* depends on the type of cultivated crop. Based on the desired maximum and minimum temperature for each level, the temperature of each level of farm f at time t is limited in constraint (6c). The electricity demand of the air conditioning system is a non-negative variable. Thus, it is the sum of the real power demand of the cooling and heating modes of the air conditioning system as presented in (6d). The reactive power demand of the air conditioning system at level l of farm f depends on the power factor of the related air conditioning system, $PF_{l,f}^a$, and the real power demand of the air conditioning system as presented in (6e).

$$P_{l,f}^{X,t} + P_{l,f}^{a,t} = \frac{m_{l,f}^a C_a (\theta_{l,f}^t - \theta_{l,f}^{t-1})}{\eta_a^f} : \lambda_{l,f}^{P_a,t} \quad (6a)$$

$$P_{l,f}^{X,t} = K_{l,f}^w A_{l,f}^w (\theta_{out}^t - \theta_{l,f}^t)/X_{l,f}^w : \lambda_{l,f}^{P_o,t} \quad (6b)$$

$$\underline{\theta}_{l,f} \le \theta_{l,f}^t \le \overline{\theta}_{l,f} : \underline{\mu}^{\theta_l^{f,t}}, \overline{\mu}^{\theta_l^{f,t}} \quad (6c)$$

$$P_{l,f}^{a,t} = P_{l,f}^{a,t,+} - P_{l,f}^{a,t,-} : \lambda_{l,f}^{pn,t} \quad (6d)$$

$$Q_{l,f}^{a,t} = \frac{\sqrt{1 - {PF_{l,f}^a}^2}}{PF_{l,f}^a} (P_{l,f}^{a,t,+} + P_{l,f}^{a,t,-}) : \lambda_{l,f}^{Q_a,t} \quad (6e)$$

3) Irrigation system: The model of the irrigation system of farm f at time t is suggested in (7). The required hours for irrigation of crops of *VF* f is limited in (7a). The electricity demand of the irrigation and fertilization systems of farm f at time t depends on the quantity of water required in each irrigation period, the height of the farm, and the efficiency of the water pumps, as shown in (7b). The reactive power demand of the irrigation system of each farm depends on the power factor of pumps utilized on the farm, PF_{ir}^{f}, and the real power demand of the irrigation system as shown in (7c).

$$\sum_{t\in\mathcal{T}} I_f^{ir,t} = \tau_{ir}^f \tag{7a}$$

$$0 \le P_{f,ir}^t = (\frac{m_w^f g \Delta_h^f}{\tau_{ir}^f T_h \eta_p^f} + \sum_{l\in\mathcal{L}_f} p_{l,f}^t) I_f^{ir,t} \quad : \underline{\mu}_{f,t}^{P_{ir}}, \lambda_{f,t}^{P_{ir}} \tag{7b}$$

$$Q_{f,ir}^t = \frac{\sqrt{1-{PF_{ir}^f}^2}}{PF_{ir}^f} P_{f,ir}^t \quad : \lambda_{f,t}^{Q_{ir}} \tag{7c}$$

4) Dehumidification system: Since VFs are indoor facilities full of crops, the absolute humidity of the air increases due to evaporated water from the crops. Thus, the de/humidification system only works in dehumidification mode. The model of the dehumidification system of level l of farm f is modeled in (8). The electricity demand of the dehumidification system of level l of farm f at time t, $P_{l,f}^{h,t}$, depends on the evaporated water from crops, and the required electricity demand of the dehumidification system to remove 1 liter water from the air as presented in (8a). The absolute humidity of each level of farm f at time t, $\varsigma_{l,f}^t$, is limited in (8b).

$$P_{l,f}^{h,t} - W_{l,f}^{e,t} p_w = (\varsigma_{l,f}^t - \varsigma_{l,f}^{t-1}) p_w \quad : \lambda_{l,f}^{P_h,t} \tag{8a}$$

$$\underline{\varsigma}_{l,f} \le \varsigma_{l,f}^t \le \overline{\varsigma}_{l,f} \quad : \underline{\mu}^{\varsigma_l^{f,t}}, \overline{\mu}^{\varsigma_l^{f,t}} \tag{8b}$$

C. EV *Charging and* DER *Model*

The solar generation power at time t is limited by the available solar power at time t as presented in (9) and is adopted from [29]

$$0 \le P_s^t \le \overline{p}_s^t \quad : \underline{\mu}_t^s, \overline{\mu}_t^s \tag{9}$$

The real power charging of fleet of *EV*s e at time t, $P_{e,t}^c$, is capped by the multiplication of the maximum charging power of fleet of *EV*s e and the ratio of connected *EV*s in the fleet (10a). The energy balance of fleet of *EV* e at time t depends on the real power charging, efficiency of the inverter, and traveling power consumption of the fleet at each time as presented in (10b). The energy of fleet of *EV*s e at time t is limited as shown in (10c) and is adopted from [29]

$$0 \le P_{e,t}^c \le \overline{p_e^c} R_c^t \quad : \underline{\mu}_{c,t}^e, \overline{\mu}_{c,t}^e \tag{10a}$$

$$E_e^t = E_e^{t-1} - (p_{e,t}^{tr} R_d^t - \gamma_e^c P_{e,t}^c) \quad : \lambda_e^t \tag{10b}$$

$$\underline{E}_e \le E_e^t \le \overline{E}_e \quad : \underline{\mu}_t^e, \overline{\mu}_t^e \tag{10c}$$

D. Distribution Network Model

The real and reactive nodal balance equations in their AC form are presented in (11a) and (11b), respectively. The real and reactive power flow constraints of line (i,j) of the *ADN* in their AC form are presented in (11c) and (11d), respectively and are adopted from [30].

$$\sum_{s\in\mathcal{S}_i} P_s^t + \sum_{g\in\mathcal{G}_i} P_g^t = \sum_{d\in\mathcal{D}_i} p_D^t + \sum_{f\in\mathcal{F}_i} P_f^t + \sum_{e\in\mathcal{E}_i} P_{e,t}^c + (G_{ii} + \sum_{j\in\delta_i} G_{ij})((e_i^t)^2 + (f_i^t)^2) + \sum_{j\in\delta_i} P_{ij}^t \tag{11a}$$

$$\sum_{g\in\mathcal{G}_i} Q_g^t = \sum_{d\in\mathcal{D}_i} q_D^t + \sum_{f\in\mathcal{F}_i} Q_f^t + \sum_{j\in\delta_i} Q_{ij}^t - (B_{ii} + \sum_{j\in\delta_i} B_{ij})[(e_i^t)^2 + (f_i^t)^2] \tag{11b}$$

$$P_{ij}^t = -G_{ij}({e_i^t}^2 + {f_i^t}^2) + G_{ij}(e_i^t e_j^t + f_i^t f_j^t) - B_{ij}(e_i^t f_j^t - e_j^t f_i^t) \tag{11c}$$

$$Q_{ij}^t = B_{ij}({e_i^t}^2 + {f_i^t}^2) - B_{ij}(e_i^t e_j^t + f_i^t f_j^t) - G_{ij}(e_i^t f_j^t - e_j^t f_i^t) \tag{11d}$$

The AC nodal balance and power flow equations have bi-linear terms that make the robust optimization problem a non-convex optimization problem. A set of *SOCP* lifting variables is introduced in (12) to relax these bi-linear terms.

$$c_{ii}^t := (e_i^t)^2 + (f_i^t)^2; \;\; c_{ij}^t := e_i^t e_j^t + f_i^t f_j^t; \;\; s_{ij}^t := e_j^t f_i^t - f_j^t e_i^t \tag{12}$$

The *SOCP* relaxed form of the nodal balance and power flow equations is presented in (13) by leveraging the *SOCP* lifting variables introduced in (12). As the *SOCP* relaxation method is tight for acyclic radial distribution networks [31], [30], the rendered solution of the optimal operation scheduling problem for the *ADN*s is exact.

$$\sum_{s\in\mathcal{S}_i} P_s^t + \sum_{g\in\mathcal{G}_i} P_g^t = \sum_{d\in\mathcal{D}_i} p_D^t + \sum_{f\in\mathcal{F}_i} P_f^t + \sum_{e\in\mathcal{E}_i} P_{e,t}^c + (G_{ii} + \sum_{j\in\delta_i} G_{ij}) c_{ii}^t + \sum_{j\in\delta_i} P_{ij}^t \quad : \lambda_i^{P,t} \tag{13a}$$

$$\sum_{g\in\mathcal{G}_i} Q_g^t = \sum_{d\in\mathcal{D}_i} q_D^t + \sum_{f\in\mathcal{F}_i} Q_f^t - (B_{ii} + \sum_{j\in\delta_i} B_{ij}) c_{ii}^t + \sum_{j\in\delta_i} Q_{ij}^t \quad : \lambda_i^{Q,t} \tag{13b}$$

$$P_{ij}^t = -G_{ij} c_{ii}^t + G_{ij} c_{ij}^t + B_{ij} s_{ij}^t \quad : \lambda_{ij}^{p,t} \tag{13c}$$

$$Q_{ij}^t = B_{ij} c_{ii}^t - B_{ij} c_{ij}^t + G_{ij} s_{ij}^t \quad : \lambda_{ij}^{q,t} \tag{13d}$$

The relationship between the *SOCP* lifting variables, and the second-order cone relaxation of the relating the *SOCP* lifting terms are presented in (14a) and (14b), respectively. Besides, the *SOCP* relaxed form of the voltage limits of each bus is presented in (14c).

$$c_{ij} = c_{ji} \quad , \quad s_{ij} = -s_{ji} \quad : \lambda_{ij}^{c,t}, \lambda_{ij}^{s,t} \tag{14a}$$

$$\left\| \begin{matrix} 2c_{ij}^t \\ 2s_{ij}^t \\ c_{ii}^t - c_{jj}^t \end{matrix} \right\| \le c_{ii}^t + c_{jj}^t \quad : \mu_{ij}^{c,t}, \mu_{ij}^{s,t}, \mu_{ij}^{cc,t}, \mu_{ij}^{cone,t} \tag{14b}$$

$$\underline{V}_i{}^2 \le c_{ii}^t \le \overline{V}_i{}^2 \quad : \underline{\mu}_{v_i}^t, \overline{\mu}_{v_i}^t \tag{14c}$$

The uncertainty of the available power of solar generation unit s at time t and the uncertainty of demand d at time t are limited by (15a)-(15b), respectively.

$$\overline{p}_s^t \in [\overline{p}_s^{t,0} - \Delta_p^{s,t}, \overline{p}_s^{t,0} + \Delta_p^{s,t}] \tag{15a}$$

$$p_D^t \in [p_D^{t,0} - \Delta_p^{d,t}, p_D^{t,0} + \Delta_p^{d,t}] \tag{15b}$$

III. Solution Method

The *SOCP* relaxed form of the optimal operation scheduling problems presented in Section II are two-stage robust optimization problems. Here, the Column-and-Constraint Generation Algorithm (C&CGA) [32] is leveraged to tackle the uncertainty of demand and available solar generation. The relaxed form of the optimal operation scheduling of *VF*s problems is presented in the compact form of the two-stage robust optimization problem, where x is the first-stage binary decision variable, y is the second-stage continuous decision variable, and u is uncertain variable realized in the second-stage problem. In Section III-B, $c, e, b, A, E, d, F, G, h, H$ are corresponding known coefficient vectors or matrices. The binary decision variables of the first-stage problem, x, are vectorized representations of the status of the lighting and irrigation systems of each floor at each time slot as presented in (5b) and (7a), respectively. The objective function (1), (2), or (3) is presented as (16a) and the sets of constraints given in (16b) and (16c) present all constraints with binary decision variables (i.e., first stage binary variables, x) that were formulated in (5a)-(5b) and (7a)-(7b). The set of constraints presented in (16c) captures the second-stage decision variables y vectorized for all indices as well as the realization of uncertain variables u such as demand of power system and solar generation availability and vectorized for all indices. The set of constraints given as (16d) presents the feasibility set of second-stage decision variables.

$$\min_{x} \quad c^T x + \max_{u \in U} (\min_{y} \quad b^T y) \tag{16a}$$

$$s.t. \quad Ax + Ey = d, x_i \in \{0,1\} \tag{16b}$$

$$Fx + Gy \geq h - Hu, x_i \in \{0,1\} \tag{16c}$$

$$y \in \Omega(x,u) \tag{16d}$$

Enumerating all scenarios with the different realizations of u is practically challenging. Therefore, to solve the problem presented in (16), an iterative solution method that selects a subset of uncertain variables at each iteration is presented. The size of the subset at each iteration is determined by the BoU. The dual form of the SOCP relaxed representation of the second-stage problem is utilized to determine the worst-case realization in an iteration given the rendered first-stage decisions from the current iteration of the algorithm. The details of the algorithm are discussed in Section III.B. The presented C&CGA determines significant scenarios that contribute to the worst realization of the system operation cost or carbon emissions. After the decomposition, the problem consists of a first-stage problem and the second-stage problem, which are shown in (17) and (18), respectively. It should be noted that ψ represents the iteration index.

$$\min_{x} \quad c^T x + \gamma \tag{17}$$

$$s.t. \quad \gamma \geq b^T y^{(\psi)}$$
$$Ax + Ey^{(\psi)} = d$$
$$Fx + Gy^{(\psi)} \geq h - Hu^{*(\psi)}$$
$$\forall x \in \Omega_x, y \in \Omega_y$$

$$\max_{u \in U} (\min_{y \in \Omega(x,u)} \quad b^T y) \tag{18}$$

$$s.t. \quad Ax + Ey^{(\psi)} = d$$
$$Fx^* + Gy \geq h - Hu$$

Here-and-now decision variables of the first-stage problem are passed through the second-stage problem. The *SOCP* relaxed inner minimization problem of the second-stage problem is reformulated as a maximization problem using its dual form. Therefore, the maximization problem presented in (19)-(27j), will render the worst realization of uncertain variables given the minimization of the inner problem. In an iterative process, the realized uncertainties are added as a column to the first-stage problem to update here-and-now decision variables. Once the CCGA algorithm is converged, no new column will be added and the final robust here-and-now decision variables are revealed.

A. Dual Reformulation of SOCP Relaxed Second-Stage Problem

To reformulate the max-min problem in the second-stage problem as a maximization problem, the dual representation of the inner minimization problem is proposed in (19)-(27) assuming that the worst realization of uncertainties occurs at the extreme point within the polyhedral uncertainty set. Note that the variable after each colon in front of dual constraints shows the related primal variables. The objective of the dual problem is presented in (19). Note that the status of the lighting system and irrigation system (i.e., $I_{l,f}^{*li,t}$ and $I_{l,f}^{*ir,t}$) are fixed based on the obtained values by solving the first-stage problem.

$$\max_{U_s^t, V_s^t, U_d^t, V_d^t} \sum_{t \in \mathcal{T}} \Bigg[\sum_{e \in \mathcal{E}} (-\overline{\mu}_{c,t}^e \overline{p_e^c} R_c^t + \underline{\mu}_t^e \underline{E}_e - \overline{\mu}_t^e \overline{E}_e - p_{e,t}^{tr} R_d^t \lambda_e^t)$$

$$+ \sum_{f \in \mathcal{F}} \sum_{l \in \mathcal{L}_f} \Bigg(K_{l,f}^w A_{l,f}^w \theta_{out}^t \lambda_{l,f}^{P_o,t} / X_{l,f}^w + \underline{\mu}^{\theta_l^{f,t}} \underline{\theta}_{l,f} - \overline{\mu}^{\theta_l^{f,t}} \overline{\theta}_{l,f} +$$

$$\underline{\mu}^{\varsigma_l^{f,t}} \underline{\varsigma}_{l,f} - \overline{\mu}^{\varsigma_l^{f,t}} \overline{\varsigma}_{l,f} + W_{l,f}^{e,t} p_w \lambda_{l,f}^{P_h,t} + \frac{A_l^f i_l^f}{\epsilon_l} I_{l,f}^{*li,t} \lambda_{f,t}^{P_{li}} \lambda_{l,f}^{P_h,t} +$$

$$I_f^{*ir,t} \lambda_{f,t}^{P_{ir}} \left(\frac{m_w^f g \Delta_h^f}{\tau_{ir}^f T_h \eta_p^f} + \sum_{l \in \mathcal{L}_f} p_{l,f}^t \right) \Bigg) + \sum_{i \in \mathcal{I}} \Bigg(\underline{\mu}_{v_i}^t \underline{V}_i{}^2 - \overline{\mu}_{v_i}^t \overline{V}_i{}^2 +$$

$$\sum_{D \in \mathcal{D}_i} \lambda_i^{P,t} p_D^{t,0} (1 + \Delta_p^{d,t} U_d^t - \Delta_p^{d,t} V_d^t) + \lambda_i^{Q,t} \sum_{d \in \mathcal{D}_i} q_D^t \Bigg) +$$

$$\sum_{s \in \mathcal{S}} \overline{\mu}_t^s \overline{p}_s^{t,0} (1 + \Delta_p^{s,t} U_s^t - \Delta_p^{s,t} V_s^t) \Bigg] \tag{19}$$

The dual constraints associated with the real power generated by solar generation unit s at time t is given in (20).

$$\underline{\mu}_t^s - \overline{\mu}_t^s + \sum_{i \in \mathcal{I}_s} \lambda_i^{P,t} = 0 \qquad : P_s^t \tag{20}$$

The dual constraints associated with the real charging power and energy of the fleet of *EV* e at time t are presented in (21a) and (21b), respectively.

$$\underline{\mu}_{c,t}^e - \overline{\mu}_{c,t}^e + \lambda_e^t - \lambda_i^{P,t} = 0 \qquad : P_{e,t}^c \tag{21a}$$

$$\underline{\mu}_e^t - \overline{\mu}_e^t + \lambda_e^t - \lambda_e^{t+1} = 0 \quad : E_e^t \quad (21b)$$

The dual constraints related to the total real and reactive power demand of the *VF* f at time t are presented in (22a) and (22b), respectively.

$$\lambda_P^{f,t} - \sum_{i \in \mathcal{I}_f} \lambda_i^{P,t} \leq 0 \quad : P_f^t \quad (22a)$$

$$\lambda_Q^{f,t} - \sum_{i \in \mathcal{F}_i} \lambda_i^{Q,t} = 0 \quad : Q_f^t \quad (22b)$$

The dual constraints associated with the lighting, air conditioning, irrigation, and humidification systems are presented in (23)-(26b). The dual constraint corresponding to the real power demand of the lighting system of *VF* f at time t is presented in (23).

$$\underline{\mu}_{f,t}^{P_{li}} + \lambda_{f,t}^{P_{li}} - \lambda_P^{f,t} = 0 \quad : P_{f,li}^t \quad (23)$$

The dual constraints related to the total real and reactive demand of the air conditioning system at level l of farm f at time t are presented at (24a) and (24b), respectively. Besides, the dual constraints corresponding to non-negative demand of the air conditioning system working in cooling and heating mode at level l of farm f at time t are presented at (24c) and (24d), respectively. The dual constraints associated with exchange heating power and temperature of l of farm f at time t are presented in (24e) and (24f), respectively.

$$\lambda_{l,f}^{P_a,t} + \lambda_{l,f}^{pn,t} = 0 \quad : P_{l,f}^{a,t} \quad (24a)$$

$$\lambda_{l,f}^{Q_a,t} - \lambda_Q^{f,t} = 0 \quad : Q_{l,f}^{a,t} \quad (24b)$$

$$-\lambda_P^{f,t} - \lambda_{l,f}^{pn,t} - \frac{\sqrt{1 - PF_{l,f}^{a\ 2}}}{PF_{l,f}^a} \lambda_{l,f}^{Q_a,t} \leq 0 \quad : P_{l,f}^{a,t,+} \quad (24c)$$

$$-\lambda_P^{f,t} + \lambda_{l,f}^{pn,t} - \frac{\sqrt{1 - PF_{l,f}^{a\ 2}}}{PF_{l,f}^a} \lambda_{l,f}^{Q_a,t} \leq 0 \quad : P_{l,f}^{a,t,-} \quad (24d)$$

$$\lambda_{l,f}^{P_a,t} + \lambda_{l,f}^{P_o,t} = 0 \quad : P_{l,f}^{X,t} \quad (24e)$$

$$\frac{m_{l,f}^a C_a}{\eta_a^f}(\lambda_{l,f}^{P_a,t+1} - \lambda_{l,f}^{P_a,t}) + \frac{K_{l,f}^w A_{l,f}^w}{X_{l,f}^w} \lambda_{l,f}^{P_o,t} + \underline{\mu}^{\theta_l^{f,t}} - \overline{\mu}^{\theta_l^{f,t}} = 0 \quad : \theta_{l,f}^t \quad (24f)$$

The dual constraints related to the total real and reactive demand of the irrigation system at level l of farm f at time t are presented at (25a), (25b), respectively.

$$\lambda_{f,t}^{P_{ir}} + \underline{\mu}_f^{P_{ir},t} - \lambda_P^{f,t} - \frac{\sqrt{1 - PF_{ir}^{f\ 2}}}{PF_{ir}^f} \lambda_{f,t}^{Q_{ir}} = 0 \quad : P_{f,ir}^t \quad (25a)$$

$$\lambda_{f,t}^{Q_{ir}} - \lambda_Q^{f,t} = 0 \quad : Q_{f,ir}^t \quad (25b)$$

The dual constraints related to the absolute humidity and demand of the dehumidification system at level l of farm f at time t are presented at (26a), (26b), respectively.

$$p_w(\lambda_{l,f}^{P_h,t+1} - \lambda_{l,f}^{P_h,t}) + \underline{\mu}^{\varsigma_l^{f,t}} - \overline{\mu}^{\varsigma_l^{f,t}} = 0 \quad : \varsigma_{l,f}^t \quad (26a)$$

$$\lambda_{l,f}^{P_h,t} - \lambda_P^{f,t} \leq 0 \quad : P_{l,f}^{h,t} \quad (26b)$$

The dual constraints associated with the real and reactive power dispatch of the feeder bus for the carbon emissions minimization problem are presented in (27a) and (27b), respectively. It should be noted that the right-hand side of the dual constraint associated with the real power dispatch of the feeder bus (27a) would be α_t if the objective is to minimize the operation cost of the distribution network. The dual constraints associated with the lifting terms c_{ii}^t, c_{ij}^t, and s_{ij}^t are given in (27c)-(27e), respectively. The dual constraints associated with real and reactive power flow of lines are presented in (27f) and (27g), respectively. The dual SOC cone is presented in (27h). To determine the worst realization of the uncertain variables, binary variables $U_s^t, V_s^t, U_d^t, V_d^t$ are introduced. Each pair of binary variables are mutually exclusive as shown in (27i). Moreover, the budget of uncertainty limits the combination of the binary variables that yields the worst realization of the uncertain variables as shown in (27j). Note that $|\mathcal{T}|(|\mathcal{S}|+|\mathcal{D}|)$ represents the total number of uncertain variables.

$$\lambda_i^{P,t} = \sum_{z \in \mathcal{Z}} C_E^{z,t} \rho_z^t \qquad \forall i \in \mathcal{I}_g \quad : P_g^t \quad (27a)$$

$$\lambda_i^{Q,t} = 0 \qquad \forall i \in \mathcal{I}_g \quad : Q_g^t \quad (27b)$$

$$(G_{ij}\lambda_{ij}^{p,t} - B_{ij}\lambda_{ij}^{q,t} - (G_{ii} + \sum_{j \in \delta_i} G_{ij})\lambda_i^{P,t} + (B_{ii} + \sum_{j \in \delta_i} B_{ij})\lambda_i^{Q,t} + \underline{\mu}_{v_i}^t - \overline{\mu}_{v_i}^t + \sum_{j \in \delta_i}(\mu_{ij}^{cc,t} + \mu_{ij}^{cone,t}) + \sum_{j \in \delta_i}(-\mu_{ji}^{cc,t} + \mu_{ji}^{cone,t}) = 0 \quad : c_{ii}^t \quad (27c)$$

$$-G_{ij}\lambda_{ij}^{p,t} + B_{ij}^{q,t}\lambda_{ij}^{q,t} + \lambda_{ij}^{c,t} - \lambda_{ji}^{c,t} + 2\mu_{i,j}^{c,t} = 0 \quad : c_{ij}^t \quad (27d)$$

$$-B_{ij}\lambda_{ij}^{p,t} - G_{ij}\lambda_{ij}^{q,t} + \lambda_{ij}^{s,t} + \lambda_{ji}^{s,t} + 2\mu_{i,j}^s = 0 \quad : s_{ij}^t \quad (27e)$$

$$-\sum_{i \in \mathcal{FB}_{ij}} \lambda_i^{p,t} + \lambda_{ij}^{p,t} = 0 \quad : P_{ij}^t \quad (27f)$$

$$-\sum_{i \in \mathcal{FB}_{ij}} \lambda_i^{q,t} + \lambda_{ij}^{q,t} = 0 \quad : Q_{ij}^t \quad (27g)$$

$$\left\| \begin{matrix} \mu_{ij}^{c,t} \\ \mu_{ij}^{s,t} \\ \mu_{ij}^{cc,t} \end{matrix} \right\| \leq \mu_{ij}^{cone,t} \quad (27h)$$

$$\begin{cases} U_s^t + V_s^t \leq 1 \\ U_d^t + V_d^t \leq 1 \end{cases} \quad (27i)$$

$$\frac{\sum_{t \in \mathcal{T}}(\sum_{s \in \mathcal{S}} U_s^t + V_s^t + \sum_{d \in \mathcal{D}} U_d^t + V_d^t)}{|\mathcal{T}|(|\mathcal{S}| + |\mathcal{D}|)} \leq BoU \quad (27j)$$

B. Column-and-Constraint Generation Algorithm

By utilizing the dual reformulation of the inner minimization problem of the second-stage problem (18) which is presented in (19)-(27j), the second-stage optimization problem is reformulated and presented in its compact form in (28).

$$\begin{aligned} \max_{u,\lambda,\mu} \quad & d^T\lambda - (h - Hu)^T\mu \\ s.t. \quad & A^T\lambda + E^T\mu = 0 \\ & \mu \geq 0 \end{aligned} \quad (28)$$

The binary-to-continuous variable multiplications in (19) are linearized using the method presented in [32]. The C&CGA that was utilized to solve the optimal scheduling problems of *VF*s is presented in Algorithm 1.

Algorithm 1 Column-and-Constraint Generation

1: Set $LB = -\infty, UB = \infty$, initialize u^0
2: $\psi = 0$
3: **while** $\frac{UB-LB}{UB} > \epsilon$ **do**
4: Using $u^{(\psi)}$ solve the first-stage prob. (17) $\rightarrow x^*, \gamma^*$
5: Set $LB = c^T x^* + \gamma^*$
6: Using x^* solve the second-stage prob. (28) $\rightarrow u^*, y^*$
7: Set $UB = c^T x^* + b^T y^*$
8: Update $\psi += 1$
9: Assign $u^{(\psi)} = u^*$
10: **end while**

In the first step, the lower bound (LB) and upper bound (UB) are set to $-\infty$ and ∞, respectively. Besides, the initial value of uncertain binary variables is set to zero. If the convergence condition is not satisfied, solving the master problem (17) procures the optimal scheduling solution for *VF*s ($I_{l,f}^{*li,t}, I_f^{*ir,t}$). The LB is updated based on the solution of the first-stage problem. In the next step, the second-stage problem (28) is solved to procure the subset of the worst-case scenario (i.e., $U_s^{*(\psi+1),t}, V_s^{*(\psi+1),t}, U_d^{*(\psi+1),t}, V_d^{*(\psi+1),t}$). Then, the upper bound of the algorithm is updated using the binary and continuous decision variables procured by solving the second-stage problem. At last, the iteration index, ψ, and $u^{(\psi)}$ will be updated. The algorithm will converge once the difference between the upper and lower bounds of the algorithm divided by the upper bound is equal or less than a small non-negative parameter (ϵ) as presented in line 3 of Algorithm 1. Once converged, the first-stage decisions procured in the last iteration are reported as here-and-now decisions. Problems (17) and (28) are *MISOCP* optimization problems, and they are solved using off-the-shelf conic programming solvers such as Gurobi [33]. Here, a PC is utilized with a Core i7 CPU 4.70 GHz processor, and 48 GB memory.

IV. Case Studies

In this section, the performance of *VF*s as a demand-responsive load is evaluated for different scenarios. Besides, the challenges and opportunities of utilizing *VF*s in the ADN are illustrated in the cases. The capability of *VF*s to increase the dispatchability of *DER*s in an *ADN* with a high penetration level of solar generation units is also demonstrated. Lastly, the coordination of *VF*s with renewable *DER*s is investigated to mitigate the impact of renewable uncertainties on ADN operation.

A. Test System Configuration

The topology of the modified IEEE 33-bus system is presented in Fig. 2. The test system consists of 33 buses, 32 branches, 7 solar generation units, 32 loads, 4 vertical farms, and 12 *EV* charging points. The base net demand, solar generation, the share of each electricity generation resource in the generation mix of each hour, and carbon emission trends are set according to the normalized hourly data of California ISO on November 4, 2021 [34]. Given the electricity demand of the *ADN* without *VF*s (120 MWh per day), there are 4200 houses in this community, and the average household number is considered 3 [35]. Assuming that each person consumes 2.5 kg of food per day, the food consumption of the community is 31.5 tons per day. Besides, the electricity usage of a 40 level with 900 m^2 *VF* that produces 32 tons of food each day [4] is 48 MWh per day. Thus, the share of the electricity demand of *VF*s with 100% penetration level in the total electricity demand of the network is roughly 30%. In [36], it is mentioned that the average CO_2 emissions of cultivating $1kg$ crops is 1.5 metric kg (mkg) CO_2. Thus, the total carbon emissions of cultivating 31.5 tons of crops per day would be 47 metric tons (mT) per day. In [37], it is mentioned that food in the United States travels about 1500 miles to get from the farm to the consumer. Assuming the transport of $5500kg$ crops with each truck, 5 miles per gallon for refrigerated trucks, and 0.0127 mT CO_2-e emission for each gallon of diesel [38], the CO_2-e of delivering the conventional agriculture produces to this community is 21 mT CO_2-e. Thus, the total carbon emissions of producing food in the presented community using conventional farming methods is 68 mT CO_2-e. Thus, the carbon emissions of $1kg$ food for the conventional farming method is 2.16 metric kg.

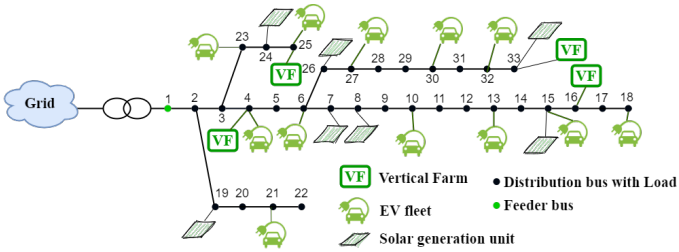

Fig. 2: Modified IEEE 33-bus test system

B. The Impact of Vertical Farming on the ADN

Here, two different objective functions are compared. In sections IV-B1 and IV-B2, the objective is to *minimize the total carbon emissions* of the distribution network over 24 hours, while the objective function in sections IV-B3 and IV-B4 is to *minimize the total operation cost* of the distribution network. To illustrate the performance of the proposed *VF* model, three cases are considered as follows.

Case 1- No *VF* is considered and the conventional agriculture fulfills the food demand

Case 2- *VF*s with inflexible demand schedule of its systems are considered within the ADN as shown in Fig. 2.

Case 3- *VF*s with shiftable demand of lighting and irrigation systems within the ADN.

It should be noted that an inflexible schedule *VF* refers to the best-practice predetermined schedule that is not flexible to changes in coordination with renewable generation.

1) Analyzing the impact of VF *on carbon emissions of food consumption and the distribution network:* Utilizing vertical farms decreases the total carbon emissions of the agriculture and transportation sectors. Here, the impact of the *VF*s on the carbon emissions of the ADN and the carbon emissions of

the transportation sector are investigated. Although electricity demand increases with the presence of *VF*s within the ADN, the overall carbon emitted by the electricity, transportation, and food sectors decreases. Shiftable demand within *VF* facilitates a further decrease in carbon emissions as it shifts *VF*'s demand into hours with a cleaner electricity generation mix. Note that the penetration level of *VF*s demonstrates the share of *VF*s in producing the total food demand in the community.

Total carbon emissions of the smart community due to agricultural activities and electricity demand of the ADN with various penetration levels of *VF*s is presented in Fig. 3. When there is no *VF*s in the community, case 1 (i.e., the penetration level of *VF*s is zero), the agricultural products are obtained from conventional agriculture methods. Fig. 3 shows that the decrease in the carbon emissions of the agriculture sector dominates the increase in the carbon emissions of the ADN with the additional *VF* demand. *Electricity Sector Case3* and *Agriculture Sector Case3* present the carbon emissions of *electricity* sector and the carbon emissions of *agriculture* sector when utilized *VF*s have shiftable demand, respectively. Exclusive community food supply by *VF*s cuts the total carbon emissions of the electricity and agriculture sectors by 62%. Fig. 3 shows that the total carbon emissions of the community in case 1 is 82.73 mT CO_2-e. It decreases 12.6% to 72.29 mT CO_2-e with a 20% supply of the community food demand by *VF*s. The maximum decrease of 66% to 28.18 mT CO_2-e is achieved in case 3 (i.e., shiftable *VF*s with 100% penetration level). The flexibility in the electricity demand of *VF*s contributed to 9% the reduction in carbon emissions when the penetration level of *VF*s is 100%. Besides, the carbon emissions of producing $1kg$ food decreased 80% from 2.18 metric k.g. CO_2-*e* in conventional agriculture to 0.43 metric kg CO_2-*e* with demand-responsive *VF*s.

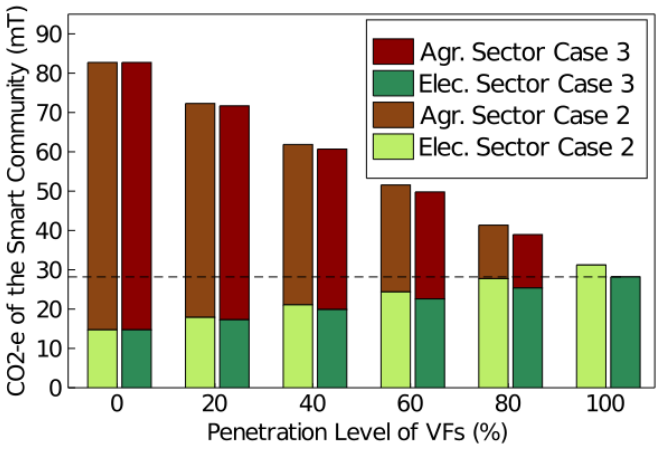

Fig. 3: Total CO_2 emissions of electricity consumption and farming activities in the smart community

Utilizing *VF*s at 100% penetration level will shift the carbon emissions of food production to the electricity sector. In Fig. 3, the emissions of the agriculture sector refer to the conventional farming emissions. At 100% penetration level of *VF*s, the food demand of the community is exclusively met by the *VF*s. As shown in Fig. 3, there is a 15 mT CO_2-e increase in emissions of the electricity sector with the increase in electricity demand of *VF*s at 100% penetration level. However, it is significantly less than 68 mT CO_2-e emissions of conventional farming in absence of *VF*s to serve the same food demand.

Fig. 4 demonstrates how *VF*s shift their demand based on the CO_2 emissions of the generation mix and the share of renewable generation units. The right Y-axis of Fig. 4 represents the CO_2 emissions associated with electricity generation, specifically the amount of carbon emitted per 10 MWh of electricity generated during the day. The CO_2 emissions of the *VF*s at time t are calculated as the product of the *VF*s' demand at time t and the CO_2-e emissions of the electricity generation at time t. In this scenario, the *VF* demand is shifted from hours with higher CO_2 emissions to those with lower CO_2 emissions. The green shaded area shows the hours with reduced demand for the shiftable *VF*s. The red shaded area demonstrates the hours with increased demand of the shiftable *VF*s. The total daily carbon emissions of inflexible schedule *VF*s is 15.03 mT CO_2-e while the one procured by shiftable *VF*s decreases 18.2% to 12.3 mT CO_2-e. Utilizing [30] to show the tightness of SOCP relaxation in constraint (14b), the minimum relaxation tightness measures for cases 1, 2, and 3 are 9.74, 9.21, and 9.54, respectively, which demonstrate a tight relaxation.

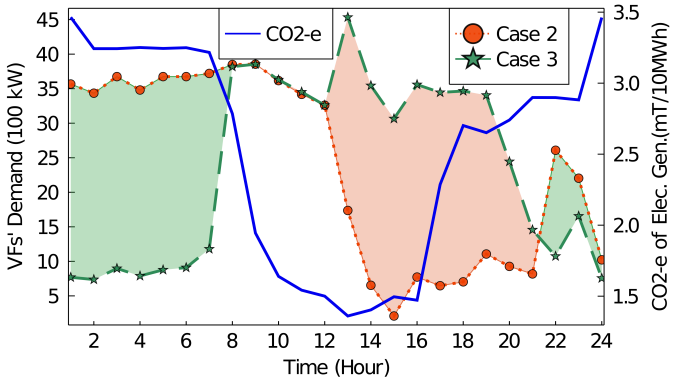

Fig. 4: Shifting the demand of *VF*s concerning CO_2 emissions

2) Demand-responsiveness of VF*s to the CO_2 emissions trend:* The presented model for *VF*s enables a flexible schedule of systems within the *VF* in response to the CO_2 emissions trends. Fig. 5 compares the performance of the shiftable *VF*s in the day during summer with one during fall, where the CO_2 emissions trends of the *VF*s are highly dependent on that of the electricity network.

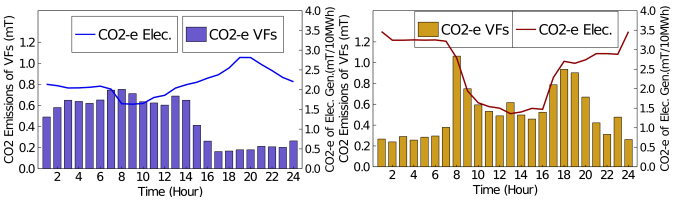

((a)) August 4, 2021 ((b)) November 4, 2021

Fig. 5: Demand-responsiveness of shiftable *VF*s

A different pattern of carbon emissions trend of electricity generation leads to different carbon emissions of 1kg food produced in *VF*s. In Table I, the carbon emissions of *VF*s, smart communities, including the electricity and agriculture sectors, and the carbon emissions of cultivating 1 kg of food are presented for different days of the year: 1) May 4th, 2021; 2) August 4th, 2021; 3) November 4th, 2021; and 4) February 4th, 2022, normalized according to the data provided by California ISO [34].

TABLE I
CARBON EMISSIONS OF THE COMMUNITY IN DIFFERENT DAYS

Day	**1**	**2**	**3**	**4**
CO_2-*e VF*s (mT)	13.41	13.57	13.67	13.65
CO_2-*e* Community (mT)	17.3	24.5	28.2	24.7
CO_2-*e* 1kg Food (mkg)	0.425	0.431	0.434	0.433

While the carbon emission of conventional farming to provide the food required in the community is 68 metric tons per day, that of *VF*s presented in Table I for different days is decreased dramatically to less than 14 metric tons per day. It is an interesting observation that *VF* enables such a reduction in carbon emissions regardless of the season. The carbon emissions of producing 1kg food from the conventional farming methods is 2.18 metric kg CO_2-*e* while the one procured by demand-responsive *VF*s is decreased more than 79% to less than 0.45 metric kg CO_2-*e* across the year. Here, the 0.45 metric kg CO_2-*e* emissions of the VFs are calculated based on the carbon emissions of the electricity generation they utilized to cultivate the crops.

3) Performance of demand-responsive VF*s in the operation cost minimization problem:* Here, the objective function of the problem is to minimize the operation cost of the electricity *ADN* as presented in (2). Here, *VF*s adjust their demand curve to minimize the operation cost of the electricity *ADN* by shifting their electricity demand to hours with lower rates. Fig. 6 a) compares the electricity demand of *VF*s procured by cost minimization and carbon emissions minimization objective functions, and Fig. 6 b) compares the carbon emissions of the *ADN* when the goal of *VF*s is minimizing the carbon emissions or the operation cost of the *ADN* for different days, where it is shown that the carbon emissions of various days of the year would be different with the cost minimization objective.

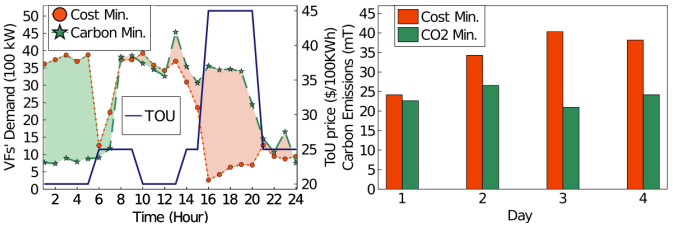

((a)) *VF*'s electricity power demand ((b)) CO_2-*e* of *ADN*

Fig. 6: the demand and carbon emissions with various choices of objective functions for Shiftable *VF*s

is

4) Enhance the dispatchability of solar generation by leveraging the flexibility of VF*s:* A high penetration level of *DER*s (e.g., 80% for solar generation units) might lead to curtailments within the *ADN* due to hosting capacity limits. Here, it is shown that utilizing *VF*s enhances dispatchability of *DER*s. Fig. 7 illustrates that the curtailed dispatch of solar generation units decreases when *VF*s are utilized in the *ADN*. The total demand of *VF*s at each hour shows that in the sunny hours of the day, *VF*s demanded more electricity to minimize the solar curtailment. The total curtailed solar dispatch procured for the cost minimization problem without *VF*s is $37.7MWh$ for 24 hours. However, the one procured for the cost minimization problem with shiftable *VF*s decreased from 71% to $10.62MWh$.

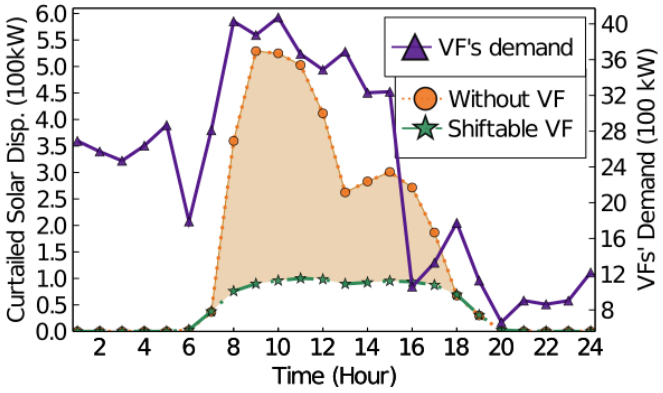

Fig. 7: The reduction in solar curtailment with shiftable *VF*s

5) The limitations of ADN*s to host* VF*s:* One major challenge of hosting *VF*s on the *ADN* is the capability of the electricity network to serve the elevated electricity demand. Fig. 8 showcases the lost load when the *VF*s with 100% penetration level are utilized to serve the demand for food of the community. Utilizing the demand-responsive *VF*s mitigates the load shedding of the *ADN* by shifting the demand. The dramatic reduction in the lost load of the *ADN* with demand-responsive *VF*s compared to the inflexible schedule is presented in Fig. 8a. The demand of the *VF*s procured by the fixed and shiftable models are compared in Fig. 8b. Thus, even with shiftable *VF*s demand, *ADN* is not ready to serve *VF*s with 100% penetration level.

The modified IEEE 33-bus system can support *VF*s with shiftable demand at 80% penetration level without load shedding. However, the *ADN* can not serve inflexible schedule *VF*s in peak hours as shown in Fig. 8c. Flexible *VF*s shifted their load to off-peak hours, as shown in Fig. 8d to prevent load shedding.

6) Joint cost and carbon emissions minimization: The joint cost and carbon emissions objective function of the optimal operation scheduling for *VF*s is proposed in (3), where the first two terms are for the first-stage problem and the last term represents the second-stage problem. Here, γ is the monetizing coefficient for carbon emissions.

$$\min_{I_{l,f}^{li,t}, I_f^{ir,t}} \sum_{t\in\mathcal{T}} \Bigg[\sum_{z\in\mathcal{Z}} (\alpha_t + \gamma C_E^{z,t} \rho_z^t) \sum_{f\in\mathcal{F}} \Bigg(\Big(\frac{m_w^f g \Delta_h^f}{\tau_{ir}^f T_h \eta_p^f} + \sum_{l\in\mathcal{L}_f} p_{l,f}^t \Big) I_f^{ir,t} + \sum_{l\in\mathcal{L}_f} \frac{A_l^f i_l^f}{\epsilon_l} I_{l,f}^{li,t} \Bigg) \Bigg] +$$

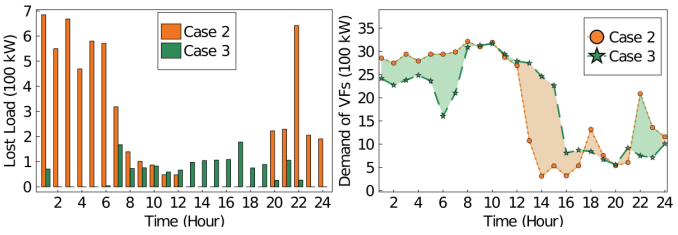

((a)) Load shedding at 100% *VF* penetration level

((b)) The demand of *VF*s at 100% penetration level

((c)) Load shedding at 80% *VF* penetration level

((d)) The demand of *VF*s at 80% penetration level

Fig. 8: The impact the shift in *VF* demand with high penetration levels on lost load within *ADN*

$$\max_{p_D^t, \overline{p}_s^t} \min_{P_g^t} \sum_{t\in\mathcal{T}} \sum_{g\in\mathcal{G}} \sum_{z\in\mathcal{Z}} (\alpha_t + \gamma C_E^{z,t} \rho_z^t) P_g^t \tag{29}$$

C. Operation Schedule of Vertical Farms Under Uncertainties

In this case, the uncertainty in demand and solar generation is considered with a deviation from the nominal values and a budget for uncertain variables over the operation horizon. Here, Algorithm 1 converges in 5 iterations with a total solve time of fewer than 30 minutes. The total carbon emissions of the smart community would increase with the introduction of uncertainties. It should be noted that all *VF*s in the ADN are considered with shiftable demand of the lighting and irrigation systems (i.e., case 3). Here, the total carbon emissions of the smart community in the presence of demand and solar generation uncertainties with 10% deviation and 10% BoU are increased to 29.98 metric tons CO_2-*e* from 28.18 metric tons CO_2-*e* without it. Fig. 9 a) illustrates that the increase in deviation and BoU results in an increase in total carbon emissions. *VF*s adjust the operating schedule of their systems to minimize the total carbon emissions of the community, taking uncertainties into account. When the deterministic case solution (i.e., the schedule of *VF*s' systems) is exposed to a stochastic case with a 5% uncertainty deviation and 20% BoU, the carbon emissions of the *VF*s increase by 30% (from 26.7 mT to 34.7 mT CO_2-e).

Fig. 9 (b) illustrates the changes in the *VF*s' schedule with uncertainty consideration,

where the *VF*s' schedule shifts towards the early morning hours due to uncertainties in both demand and solar generation units, underscoring the importance of considering these uncertainties when determining the optimal schedule for irrigation and lighting.

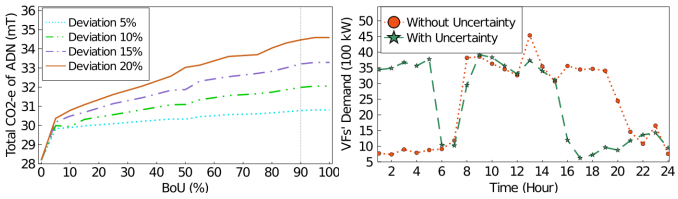

((a)) Increase in the total CO_2-e of the *ADN* under uncertainty

((b)) The shift in the schedule of *VF*s due to uncertainties

Fig. 9: Impact of uncertainties on the schedule of *VF*s and total CO_2-e of the *ADN*

Increasing the deviation of uncertain variables from nominal values increases the carbon emissions of the *ADN* as well as the smart community. Besides, the adverse impact of uncertainties is more notable in lower penetration levels of *VF*s as shown in Table II. Here, deterministic case emissions of the *VF* are compared with that of the uncertain case with 5% Deviation and 20% BoU when the penetration level of *VF*s is 10% and 80%. It is shown that the adverse impact of uncertainty is mitigated at higher penetration levels of VF.

TABLE II
MITIGATING THE ADVERSE IMPACT OF UNCERTAINTY WITH *VF*S

	10% VF's Pen. Level	**80% VF's Pen. Level**
Deterministic case emissions (mT CO_2-e)	15.14	25.6
Emissions with 5% deviation and 20% BoU (mT CO_2-e)	16.37	26.7
Adverse impact of uncertainties (%)	**8.12**	**4.43**

Adding the CO_2-e of conventional farming (the remaining 20% of the community food demand) to the total carbon emissions of the ADN procures the total carbon emissions of the community. The total carbon emissions of the community with 80% penetration level of *VF*s for deterministic and uncertain cases are 42.04 mT and 43.3 mT CO_2-e, respectively.

V. CONCLUSIONS

In this paper, the model of the electricity demand of vertical farms, as a demand-responsive asset, is presented. Coordinating *VF*s with other assets within the active distribution network (e.g., solar generation units and electric vehicles) introduces several opportunities and challenges to utilities. The preparedness of the electricity network plays a vital role in expanding vertical farms. A framework to utilize vertical farms in the active distribution network under demand and solar generation uncertainties using AC power flow constraints is presented. The proposed two-stage robust optimization problem is solved by decomposing it using the column and constraint generation algorithm. The dual presentation of the relaxed second-order cone programming problem for the inner minimization problem of the second-stage problem is presented to reformulate the second-stage problem as a maximization problem. The performance of the model in mitigating the carbon emissions of the agriculture and

electricity sectors is compared with conventional agricultural methods. Besides, the merit of utilizing vertical farms as a demand-responsive asset for grid operators is evaluated, where its coordination with other *DER*s, such as electric vehicles and solar generation units, can lead to 79% decrease in the carbon emissions of food production. Besides, shifting the demand of vertical farms to hours with a cleaner generation mix will decrease the carbon emissions of the electricity network. Moreover, it is illustrated that utilizing shiftable *VF*s contributes to a significant improvement in the dispatchability of solar generation resources. Finally, it is discussed that, although uncertainty contributes to the increase in carbon emissions, a higher penetration level of vertical farms would mitigate such an adverse impact. The suggested future work is the long-term expansion planning of vertical farms within the distribution network.

REFERENCES

[1] C. Banerjee and L. Adenaeuer, "Up, up and away! the economics of vertical farming," *Journal of Agricultural Studies*, vol. 2, no. 1, pp. 40–60, 2014.

[2] D. Despommier, "Farming up the city: the rise of urban vertical farms," *Trends in biotechnology*, vol. 31, no. 7, pp. 388–389, 2013.

[3] M. S. Mir, N. B. Naikoo, R. H. Kanth, F. Bahar, M. A. Bhat, A. Nazir, S. S. Mahdi, Z. Amin, L. Singh, W. Raja *et al.*, "Vertical farming: The future of agriculture: A review," *The Pharma Innovation Journal*, pp. 1175–1195, 2022.

[4] F. Kalantari, O. Mohd Tahir, A. Mahmoudi Lahijani, and S. Kalantari, "A review of vertical farming technology: A guide for implementation of building integrated agriculture in cities," in *Advanced Engineering Forum*, vol. 24. Trans Tech Publ, 2017, pp. 76–91.

[5] J. Wang, S. K. Vanga, R. Saxena, V. Orsat, and V. Raghavan, "Effect of climate change on the yield of cereal crops: a review," *Climate*, vol. 6, no. 2, p. 41, 2018.

[6] W. Wakeland, S. Cholette, and K. Venkat, "Food transportation issues and reducing carbon footprint," in *Green technologies in food production and processing*. Springer, 2012, pp. 211–236.

[7] G. Ares, B. Ha, and S. R. Jaeger, "Consumer attitudes to vertical farming (indoor plant factory with artificial lighting) in china, singapore, uk, and usa: A multi-method study," *Food Research International*, vol. 150, p. 110811, 2021.

[8] P. Platt, "Vertical farming: An interview with dickson despommier," *Gastronomica*, vol. 7, no. 3, pp. 80–87, 2007.

[9] M. Al-Chalabi, "Vertical farming: Skyscraper sustainability?" *Sustainable Cities and Society*, vol. 18, pp. 74–77, 2015.

[10] F. Kalantari, O. M. Tahir, R. A. Joni, and E. Fatemi, "Opportunities and challenges in sustainability of vertical farming: A review," *Journal of Landscape Ecology*, vol. 11, no. 1, pp. 35–60, 2018.

[11] W. F. Lamb, T. Wiedmann, J. Pongratz, R. Andrew, M. Crippa, J. G. Olivier, D. Wiedenhofer, G. Mattioli, A. Al Khourdajie, J. House *et al.*, "A review of trends and drivers of greenhouse gas emissions by sector from 1990 to 2018," *Environmental research letters*, 2021.

[12] N. Höhne, M. den Elzen, J. Rogelj, B. Metz, T. Fransen, T. Kuramochi, A. Olhoff, J. Alcamo, H. Winkler, S. Fu *et al.*, "Emissions: world has four times the work or one-third of the time," 2020.

[13] G. Todde, L. Murgia, M. Caria, and A. Pazzona, "A comprehensive energy analysis and related carbon footprint of dairy farms, part 2: Investigation and modeling of indirect energy requirements," *Energies*, vol. 11, no. 2, p. 463, 2018.

[14] D. Gasperi, "Urban horticulture: reducing food miles to improve cities microclimate and environmental sustainability," 2017.

[15] A. F. Soofi, S. D. Manshadi, and A. Saucedo, "Farm electrification: A road-map to decarbonize the agriculture sector," *The Electricity Journal*, vol. 35, no. 2, p. 107076, 2022.

[16] A. F. Soofi, R. Bayani, and S. D. Manshadi, "Investigating the impact of electric vehicles on the voltage profile of distribution networks," in *2022 IEEE Power & Energy Society Innovative Smart Grid Technologies Conference (ISGT)*. IEEE, 2022, pp. 1–5.

[17] B. Yu, F. Sun, C. Chen, G. Fu, and L. Hu, "Power demand response in the context of smart home application," *Energy*, vol. 240, p. 122774, 2022.

[18] H. Ming, J. Meng, C. Gao, M. Song, T. Chen, and D.-H. Choi, "Efficiency improvement of decentralized incentive-based demand response: Social welfare analysis and market mechanism design," *Applied Energy*, vol. 331, p. 120317, 2023.

[19] M. Chen, C. Gao, M. Song, S. Chen, D. Li, and Q. Liu, "Internet data centers participating in demand response: A comprehensive review," *Renewable and Sustainable Energy Reviews*, vol. 117, p. 109466, 2020.

[20] Y. Li, M. Han, Z. Yang, and G. Li, "Coordinating flexible demand response and renewable uncertainties for scheduling of community integrated energy systems with an electric vehicle charging station: A bi-level approach," *IEEE Transactions on Sustainable Energy*, vol. 12, no. 4, pp. 2321–2331, 2021.

[21] S. Baghali, Z. Guo, W. Wei, and M. Shahidehpour, "Electric vehicles for distribution system load pickup under stressed conditions: A network equilibrium approach," *IEEE Transactions on Power Systems*, 2022.

[22] G. Fan, Z. Yang, H. Jin, X. Gan, and X. Wang, "Enabling optimal control under demand elasticity for electric vehicle charging systems," *IEEE Transactions on Mobile Computing*, 2020.

[23] P. Munankarmi, J. Maguire, S. P. Balamurugan, M. Blonsky, D. Roberts, and X. Jin, "Community-scale interaction of energy efficiency and demand flexibility in residential buildings," *Applied Energy*, vol. 298, p. 117149, 2021.

[24] P. Herath and G. K. Venayagamoorthy, "Scalable residential demand response management," *IEEE Access*, vol. 9, pp. 159 133–159 145, 2021.

[25] Z. Li, Z. Sun, Q. Meng, Y. Wang, and Y. Li, "Reinforcement learning of room temperature set-point of thermal storage air-conditioning system with demand response," *Energy and Buildings*, vol. 259, p. 111903, 2022.

[26] R. Bayani, S. D. Manshadi, G. Liu, Y. Wang, and R. Dai, "Autonomous charging of electric vehicle fleets to enhance renewable generation dispatchability," *CSEE Journal of Power and Energy Systems*, 2021.

[27] V. M. Perez, *Study of the sustainability issues of food production using vertical farm methods in an urban environment within the state of Indiana*. Purdue University, 2014.

[28] S. Siebert, F. Ewert, E. E. Rezaei, H. Kage, and R. Graß, "Impact of heat stress on crop yield—on the importance of considering canopy temperature," *Environmental Research Letters*, vol. 9, no. 4, p. 044012, 2014.

[29] A. F. Soofi, R. Bayani, and S. D. Manshadi, "Analyzing power quality implications of high level charging rates of electric vehicle within distribution networks," in *2021 IEEE Transportation Electrification Conference & Expo (ITEC)*. IEEE, 2021, pp. 684–689.

[30] A. Farokhi-Soofi, S. D. Manshadi, G. Liu, and R. Dai, "A socp relaxation for cycle constraints in the optimal power flow problem," *IEEE Transactions on Smart Grid*, vol. 99, no. 4, pp. 1–10, 2020.

[31] A. Farokhi-Soofi and S. D. Manshadi, "Demand variation impact on tightness of convex relaxation approaches for the acopf problem," in *2020 52nd North American Power Symposium (NAPS)*. IEEE, 2021, pp. 1–6.

[32] S. D. Manshadi and M. E. Khodayar, "Risk-averse generation maintenance scheduling with microgrid aggregators," *IEEE Transactions on Smart Grid*, vol. 9, no. 6, pp. 6470–6479, 2017.

[33] L. Gurobi Optimization, "Gurobi optimizer reference manual," 2019.

[34] CAISO, "California iso," Available at https://www.caiso.com/Pages/default.aspx, (11/05/2021).

[35] A. Fremstad, A. Underwood, and S. Zahran, "The environmental impact of sharing: household and urban economies in co2 emissions," *Ecological economics*, vol. 145, pp. 137–147, 2018.

[36] OurWorldinData, "Greenhouse gas emissions per kilogram of food product," https://ourworldindata.org/grapher/ghg-per-kg-poore, (Accessed on 10/24/2022).

[37] Foodwise, "How far does your food travel to get to your plate?" Available at https://foodwise.org/learn/how-far-does-your-food-travel-to-get-to-your-plate/, (10/24/2022).

[38] EPA, "Greenhouse gases equivalencies calculator - calculations and references," Available at https://www.epa.gov/energy/greenhouse-gases-equivalencies-calculator-calculations-and-references, (12/20/2022).